Photochemistry and Photobiology, 2017, 93: 626–631

Research Note

Computed Regioselectivity and Conjectured Biological Activity of Ene Reactions of Singlet Oxygen with the Natural Product Hyperforin

Inna Abramova[1], Benjamin Rudshteyn[1†], Joel F. Liebman[2] and Alexander Greer[1*]

[1]Department of Chemistry, Graduate Center, City University of New York, Brooklyn College, Brooklyn, NY
[2]Department of Chemistry and Biochemistry, University of Maryland, Baltimore County, Baltimore, MD

Received 18 August 2016, accepted 16 November 2016, DOI: 10.1111/php.12706

ABSTRACT

Hyperforin is a constituent of St. John's wort and coexists with the singlet oxygen sensitizer hypericin. Density functional theory, molecular mechanics and Connolly surface calculations show that accessibility in the singlet oxygen "ene" reaction favors the hyperforin "southwest" and "southeast" prenyl (2-methyl-2-butenyl) groups over the northern prenyl groups. While the southern part of hyperforin is initially more susceptible to oxidation, up to 4 "ene" reactions of singlet oxygen can take place. Computational results assist in predicting the fate of adjacent hydroperoxides in hyperforin, where the loss of hydrogen atoms may lead to the formation of a hydrotrioxide and a carbonyl instead of a Russell reaction.

INTRODUCTION

Prenylated compounds such as hyperforin are constituents of St. John's wort (1–10) (Fig. 1). The natural photosensitizer hypericin is also present in St. John's wort and upon irradiation generates singlet oxygen ($^1O_2$, refers to the $^1\Delta$ state) and so can be phototoxic (11–15). It has been shown that prenyl (2-methyl-2-butenyl) groups react with $^1O_2$ by "ene" reactions (16–21) to give secondary and tertiary allylic hydroperoxides (**3**:**4**) often in a ~1:1 ratio (20–28) (Fig. 2) as in the reaction of $^1O_2$ with prenylphenols [*o*-(2-hydroxy-3-methylbut-3-enyl) phenols] (17–19) and prenyllipids (20). We have previously reported that prenylsurfactants [$(CH_3)_2C = CH(CH_2)_nSO_3^- Na^+$ (n = 4, 6, 8)] react with $^1O_2$ by the "ene" at the air–water interface (29). In that study, we observed a regioselectivity for a secondary rather than tertiary hydroperoxide argued for an orthogonally oriented alkene relative to the water surface (29).

In spite of interest in phototoxic properties and synthesis of constituents of St. John's wort (30–35) and natural plant defense compounds (36,37), no evidence yet exists for the reaction of hyperforin with $^1O_2$ and polyhydroperoxide products that may arise. Furthermore, the total rate constant for removal of singlet oxygen (k_T) by hyperforin has not been reported. Thus, there is a need for mechanistic studies in the singlet oxygenation of hyperforin. We have used here density functional theory (DFT) and molecular mechanics to generate insights into regioselectivity of "ene" reactions between $^1O_2$ and this natural product.

Specifically, this study describes computations of (1) hyperforin keto–enol tautomerizations, (2) hyperforin uptake of $^1O_2$ and polyhydroperoxide formation, (3) Connolly surface accessibility to anticipate regioselectivity effects of the ene reaction of $^1O_2$ and the sequence of addition of $^1O_2$ molecules from "southwest" and "southeast" sites of hyperforin, and (4) pairing reactions of adjacent hydroperoxyl radicals, in which two $^1O_2$ molecules initially bind and a hydrotrioxide and carbonyl are produced.

METHODS

Density functional theory (DFT) calculations were performed with the Gaussian 09 program package (38). The B3LYP functional was used along with the D95** basis set (39). Frequency calculations established the type of stationary point obtained. Intrinsic reaction coordinate calculations demonstrated that saddle points connected minima. Monte Carlo conformational searches of hyperforin **1** were conducted with the MM+ force field using HyperChem 8.0 program (40). The range for acyclic torsion variation was set from ±60° to 180° and the range for ring torsion flexing from ±30° to 120° with the number of simultaneous variations ranging from 1 to 8. Usage-directed Metropolis criterion (DMC) search method employed a temperature of 300 K, switching to 2000 K after 15 repeated or 30 rejected conformations. Pre-optimization checks included skipping the optimization if atoms were closer than 0.5 Å and if torsions were within 15° of previous conformations. The structures were considered to be duplicates if the energy was within 0.05 kcal mol^{-1}. Optimization terminations were set with RMS gradient 0.01 kcal/(Å-mol) and with maximum cycles of 1000. The search termination limits were set to 100 000 iterations or 1000 optimizations with the limit for conformations kept set to 1000 conformations.

Connolly molecular surface areas (41,42) were generated by the tip of the solvent probe rolling around the van der Waals volume of the molecule using ChemBio3D Ultra 13.0 (43) and GaussView 5 (44). These calculations are related to solvent-accessible areas, which have an error of 1.6 Å^2 to 3.0 Å^2 (45). Previous CCSD(T)/cc-pVTZ//B3LYP/6-311++G (2df,2p) or CCSD(T)/cc-pVTZ//B3LYP/6-311G(2d,2p) studies were successful in computing reactions of methyl (46) and ethyl peroxy radicals (47), respectively. Here, we have used B3LYP/D95** calculations which have performed well in predicting reaction enthalpies of peroxy radicals (46,47). The closed-shell method of calculation was adopted because unrestricted calculations for transition states of Russell reaction could result in high spin contamination as found often in diradicals (46). Singlet oxygen energy was calculated by adding to the energy of ground-state oxygen 22.5 kcal mol^{-1}, which is the experimentally determined triplet–singlet gap.

*Corresponding author email: agreer@brooklyn.cuny.edu (Alexander Greer)
†Present address: Department of Chemistry, Yale University, New Haven, CT 06520.

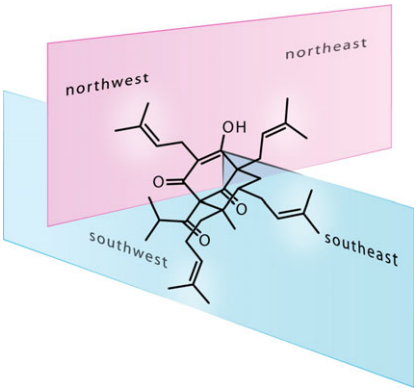

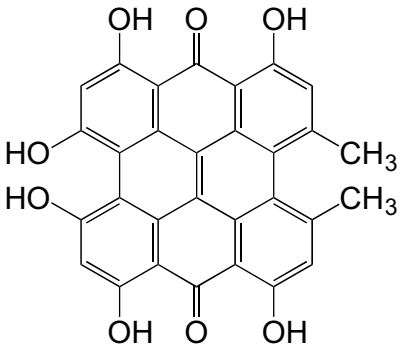

1 **2**

Figure 1. Natural products hyperforin **1** and hypericin **2**.

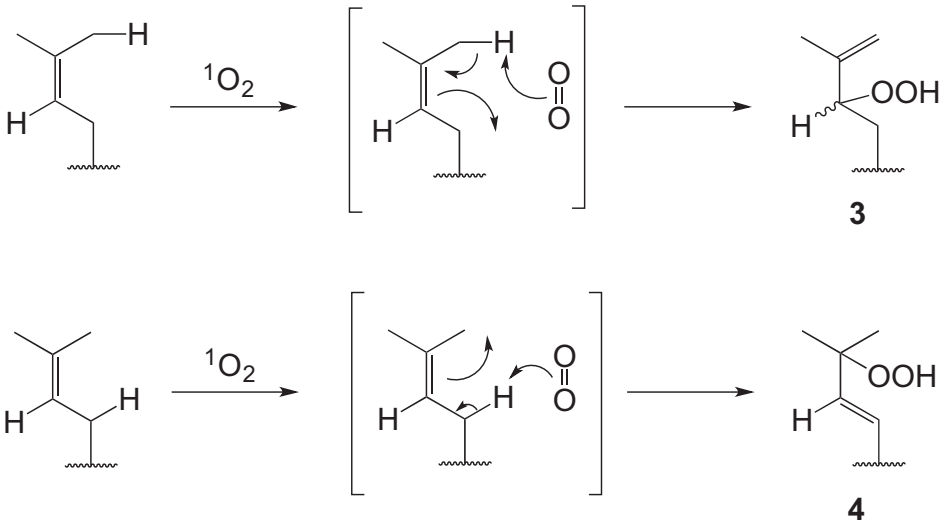

Figure 2. Ene reactions of $^1O_2$ with prenyl groups leading to a secondary hydroperoxide (**3**) and a tertiary hydroperoxide (**4**).

RESULTS AND DISCUSSION

Hyperforin keto–enol tautomerization

Mixtures of hyperforin tautomers have been implied due to broad ^{1}H NMR peaks and low resolution of ^{13}C NMR peaks (9), but little information is available on their stability. To provide additional evidence for the formation of tautomers, we have computed their relative energetics. First, we carried out a Monte Carlo conformational search of the keto form with the MM+ force field followed by B3LYP/D95** calculations of the resulting 10 lowest conformations. The lowest free energy conformer was calculated in the gas phase to determine the relative energetics between the three conformers given in Fig. 3. Enol **5** and keto **7** forms are nearly degenerate in energy and represent the global minima, where they are 1.2–1.4 kcal mol^{-1} more stable than enol **6**. While enol **6** can form a hydrogen bond, this does not lead to a more stable tautomer. Hyperforin tautomerizations are reminiscent of the monocyclic cyclohexane-1,3-dione. In the gas phase, the diketo form has been calculated to be more stable than its enol(s). The reverse stability order is found in the condensed phase because of the presence of extensive intermolecular hydrogen bonding (48,49). Because tautomers **5**–**7** are fairly close in energy, the rearrangement should be facile between them. The Cartesian coordinates for compounds **5**–**7** can be found in the Supporting Information section.

Singlet oxygen uptake and hydroperoxide formation

Here, we postulate on tandem reactions of hyperforin with singlet oxygen to reach polyhydroperoxides. In addition to the predicted formation of a secondary **3** or tertiary monohydroperoxide **4** at each of the four prenyl sites, di-, tri- and tetrahydroperoxides may also form in reaction mixtures. Each tautomer of hyperforin (**5**–**7**) provides a set of eight possible oxidation sites. Subsets can be formed solely of mono-, di-, tri- or tetrahydroperoxides. For the

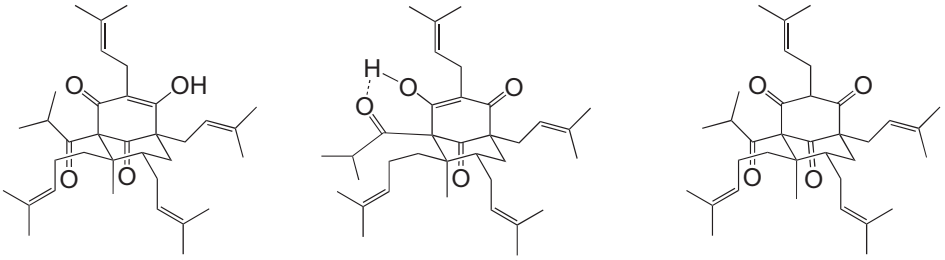

5 0 kcal/mol **6** 1.4 kcal/mol **7** 0.2 kcal/mol

Figure 3. Calculated keto–enol tautomers of hyperforin.

second singlet oxidation, six possible sites are left after eliminating the site on the peroxidized chain. Furthermore, there are many possible products of polyhydroperoxides for each tautomeric form of hyperforin (**5**-**7**). We believe there is value in computations of hyperforin—$^1O_2$ reactions due to the four prenyl reactive groups and the various mixtures of allylic hydroperoxides that could form. Thus, we now turn to the topic of computed regioselectivity of the reaction of hyperforin with $^1O_2$.

Regioselectivity of the ene reaction of singlet oxygen with hyperforin

Connolly computations (41,42) provide a tool to predict the $^1O_2$ regioselectivity in this natural product and consist of a van der Waals surface where solvent sphere makes contact. The calculations were performed with the lowest energy conformation before and after prenyl groups are replaced by a hydrogen atom. Figure 4 shows the computed surfaces where deletion of the southwest prenyl or the southeast prenyl caused the greatest decrease in area. Thus, the greatest accessible area decrease is by deletion of southwest prenyl (10.8%), followed by deletion of southeast prenyl (10.6%), and the deletion of northwest (10.1%) and northeast (9.2%) prenyls. The deletion of the southeast prenyl is pronounced, compared to the northwest and northeast prenyls, although the southwest prenyl may be competitive as it is only reduced in area by 0.2%. This suggests that the alkene groups in the southeast and southwest are the most accessible to $^1O_2$ followed by the northwest, and lastly northeast. Computations have also been carried out for a comparison to a butyl substituent series. Calculations have been used to analyze the accessible area, which differs by 3.4% as the substituent is changed from *n*-butyl to *t*-butyl in *n*-butylmethane and *t*-butylmethane, that is *n*-pentane and neopentane. This percent difference gives insight to surface area calculations as a method to quantitate steric effects.

To sum up, the formation of hydroperoxides in ene reactions of $^1O_2$ is sensitive to steric effects, where singlet oxygen avoids approach from more hindered directions (22,23). Restricted access in northeast hyperforin prenyl is modeled where formation of the tetrahydroperoxide becomes less likely.

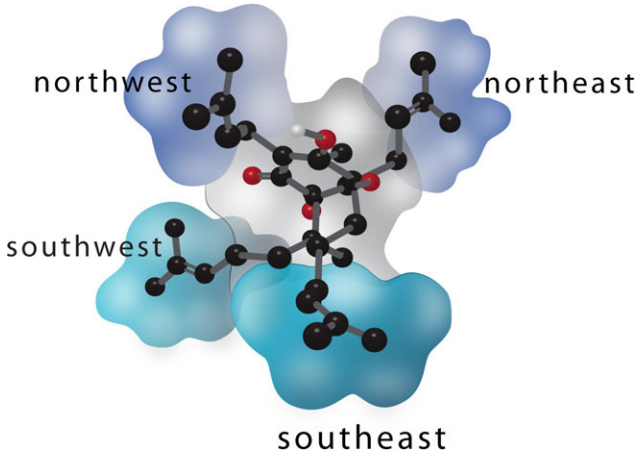

Figure 4. Connolly molecular surface calculations of the individual prenyl groups in hyperforin.

Mechanism of hydroperoxide decomposition

The addition of two $^1O_2$ molecules to the southern prenyls of hyperforin is an example where dihydroperoxide structure becomes possible as computed by DFT (Fig. 5; Cartesian coordinates for hyperforin dihydroperoxide are available in the Supporting Information section). Two secondary allylic hydroperoxides were computed, although the hyperforin core may act as a bulky group so that **4** rather than **3** would be the major product, but we did not study this computationally, that is the regioselective preference of the prenyl groups for secondary *vs* tertiary hydroperoxides. We conjecture that adjacent hydroperoxide groups will interact via loss of hydrogen atoms producing adjacent peroxyl radicals. Hydroperoxides can lose a hydrogen atom where autoxidation reactions or carbon-centered radicals or alkoxy radicals can lead to the abstraction. Russell reactions can subsequently take place by dimerization of peroxyl radicals (50–54). Here, the computations focused on methyl peroxyl radicals as a model of hyperforin peroxyl radicals to provide insight into their reactivity. Due to the excessive computer time, CPU and memory needed for a study of the U-shaped peroxy diradical, our model system has focused on methyl peroxyl radicals (Fig. 6). There are a number of transition states that may be reached in the reaction of two methyl peroxyl radicals according to B3LYP/D95** calculations of reaction enthalpies.

Five pathways were calculated. As we will see, based on computed energetics, dimerization of peroxy radicals proceeds by pathway A to form hydrotrioxide and is preferred to pathways B-D. A 12.3 kcal mol^{-1} transition structure (TS1) involved 2 CH_3O_2• to form CH_3OOOH and formaldehyde (path A, Fig. 7). A 19.0 kcal mol^{-1} saddle point (TS2) connects 2 CH_3O_2• with CH_3O• + formaldehyde + HO_2•, which represents a

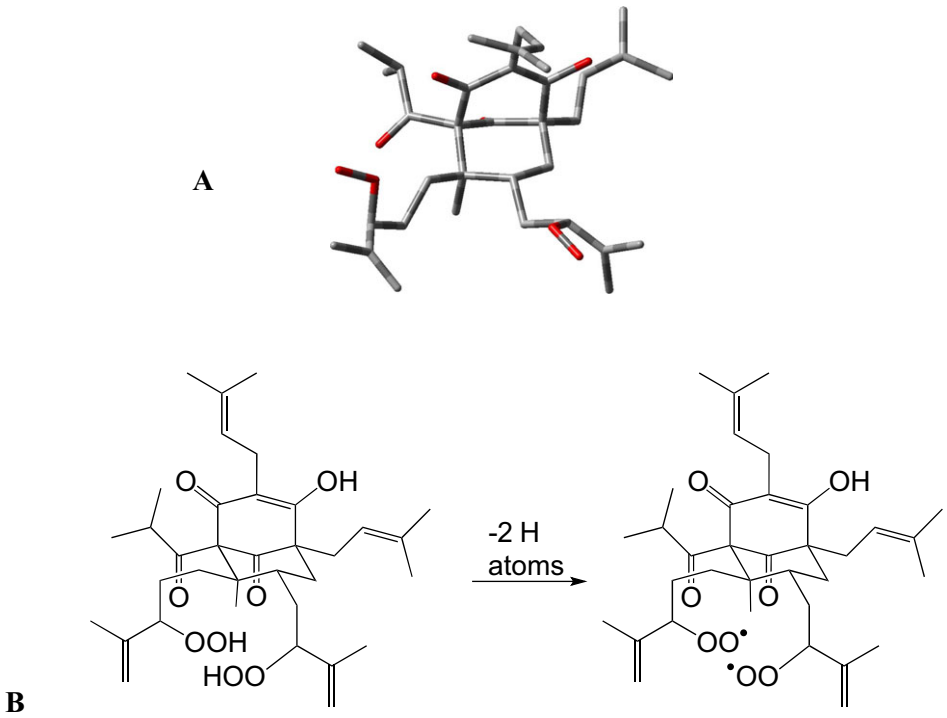

Figure 5. DFT-computed hyperforin dihydroperoxide (A) and postulated formation of adjacent peroxyl radicals (B).

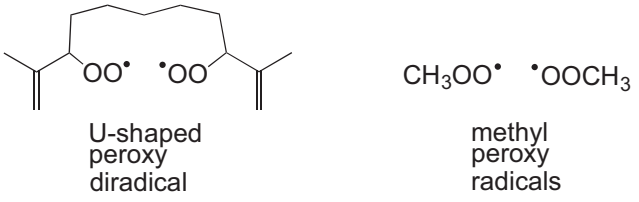

Figure 6. Calculated model systems of U-shaped region of hyperforin peroxy radicals. Possible intra- and intermolecular reactions between peroxy radical pairs.

H-abstraction by one of the methyl peroxy radicals (reaction B, Fig. 7). The results imply that there is a preference for pathway A. The enthalpy for reaction pathway A was found to be -41.1 kcal mol^{-1}, while the enthalpy for reaction pathway B to be -19.1 kcal mol^{-1}. Other minima and transition structures were found. A 22.0 kcal mol^{-1} saddle point (TS3) connects 2 CH_3O_2• with CH_3OOH + •CH_2OO• (path C, Fig. 7). Compared to the Russell reaction (path D), the barriers in pathways A-C are lower in energy. A 38.8 kcal mol^{-1} saddle point (TS4) connects 2 CH_3O_2• with CH_3OH + formaldehyde + $^1O_2$ with a correction used of $^3O_2$ + 22.5 kcal mol^{-1} (path D, Fig. 7), which is in reasonably good agreement with the CCSD(T)/cc-pVTZ//B3LYP/6-311++G(2df,2p) calculated barrier of 33.3 kcal mol^{-1} (46). Pathway E is also high in energy due to the formation of singlet oxygen, where a 63.4 kcal mol^{-1} saddle point (TS5) connects 2 CH_3O_2• with CH_3OOCH_3 and $^1O_2$ (path E, Fig. 7). In all cases except path C, the methyl peroxyl radical reagents are high-energy species compared to the products.

In closing, a question may be posed: *Why does the natural product hyperforin coexist with the $^1O_2$ sensitizer hypericin in the plant?* The answer may relate to the predicted chemical quenching of $^1O_2$ by hyperforin. A plausible similarity is the carotenoid $^1O_2$ quenching protection seen in photosynthetic centers, although this comparison of $^1O_2$ quenching by hyperforin and carotenoids is beyond the scope of the current study as it would require a calculational study of carotenoids (55–58). It is tempting to speculate that natural polyenes (hyperforin and carotenoids) quench $^1O_2$ as a protection mechanism in plants, in which hyperforin may deactivate $^1O_2$ by a combination of chemical and physical quenching to remove $^1O_2$ from the vicinity of hypericin. Future k_T measurements for the total $^1O_2$ quenching rate constants could be examined for model hyperforin compounds with variable numbers of prenyl groups to estimate the ability of polyprenyl compounds to remove $^1O_2$.

CONCLUSION

A computational study has focused on hyperforin reactions with $^1O_2$. Our Connolly surface analysis provided evidence that $^1O_2$ accessibility is likely to determine which prenyl site is oxidized. It reveals a preference for "ene" reactions with the southeast and southwest prenyls over the northeast and northwest prenyls. This is explained by the southern prenyls branching further away from the hyperforin core so that $^1O_2$ is accessible. Our theoretical data also provide evidence for the fate of the hydroperoxides. The formation of a hydrotrioxide and carbonyl compound arises from the loss of two hydrogen atoms, shown by the reaction of two methyl peroxyl radicals to model of a hyperforin dihydroperoxide.

Acknowledgements—I.A., B.R. and A.G. acknowledge support from the National Science Foundation (CHE-1464975). B.R. was the recipient of a Barry M. Goldwater Scholarship (2012-2013). This work used the Extreme Science and Engineering Discovery Environment (XSEDE),

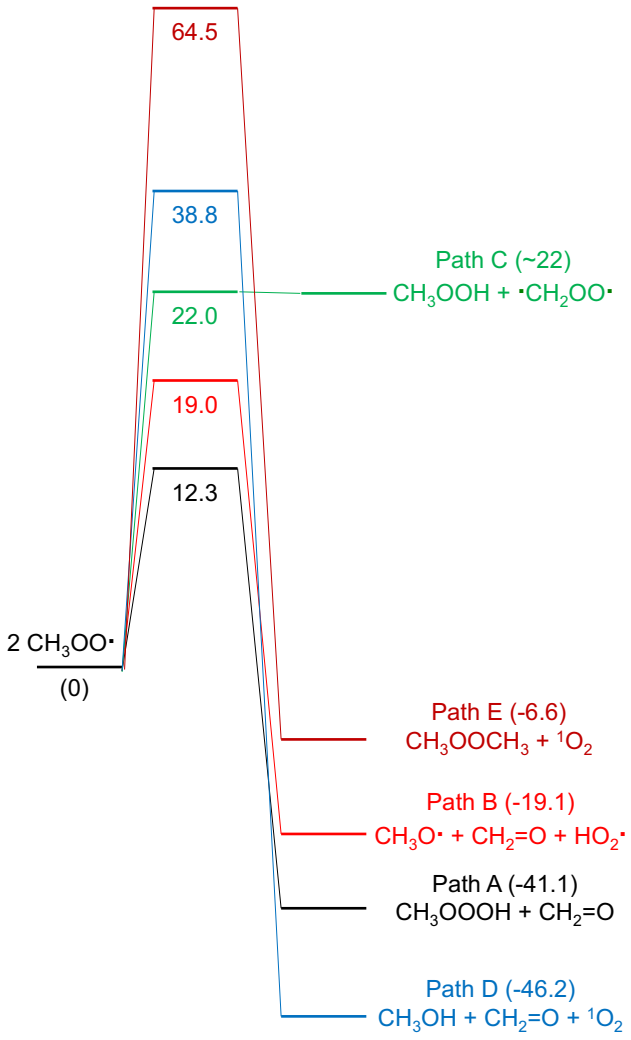

Figure 7. B3LYP/D95**-computed reactions of methyl peroxy radicals.

which is supported by National Science Foundation grant number ACI-1053575. We thank Leda Lee, Jeff Olson and Niluksha Walalawela for discussions.

SUPPORTING INFORMATION

Additional Supporting Information may be found in the online version of this article:

Table S1. Cartesian coordinates for compounds **5**, **6** and **7** and the hyperforin dihydroperoxide in Figure 5.

REFERENCES

1. Schmidt, S., G. Jürgenliemk, T. J. Schmidt, H. Skaltsa and J. Heilmann (2012) Bi-, tri-, and polycyclic acylphloroglucinols from *Hypericum empetrifolium*. *J. Nat. Prod.* **75**, 1697–1705.
2. Singh, I. P., J. Sidana, S. B. Bharate and W. J. Foley (2010) Phloroglucinol compounds of natural origin: synthetic aspects. *Nat. Prod. Rep.* **27**, 393–416.
3. Nahrstedt, A. and V. Butterweck (2010) Lessons learned from herbal medicinal products: the example of St. John's wort. *J. Nat. Prod.* **73**, 1015–1021.
4. Beerhues, L. (2006) Hyperforin. *Phytochem.* **67**, 2201–2207.
5. Fourneron, J. D. and Y. Naït-Si (2006) Effect of eluent pH on the HPLC-UV analysis of hyperforin from St. John's wort (*Hypericum perforatum* L.). *Phytochem. Anal.* **17**, 71–77.
6. Ciochina, R. and R. B. Grossman (2006) Polycyclic polyprenylated acylphloroglucinols. *Chem. Rev.* **106**, 3963–3986.
7. Vollmer, J. J. and J. Rosenson (2004) Chemistry of St. John's wort: hypericin and hyperforin. *J. Chem. Educ.* **81**, 1450–1456.
8. Adam, P., D. Arigoni, A. Bacher and W. Eisenreich (2002) Biosynthesis of hyperforin in *Hypericum perforatum*. *J. Med. Chem.* **45**, 4786–4793.
9. Verotta, L., G. Appendino, J. Jakupovic and E. Bombardelli (2000) Hyperforin analogues from St. John's wort (*Hypericum perforatum*). *J. Nat. Prod.* **63**, 412–415.
10. Repcák, M. and P. Mártonfi (1997) The localization of secondary substances in *Hypericum perforatum* flower. *Biologia* **52**, 91–94.
11. Onoue, S., Y. Seto, M. Ochi, R. Inoue, H. Ito, T. Hatano and S. Yamada (2011) In vitro photochemical and phototoxicological characterization of major constituents in St. John's Wort (*Hypericum perforatum*) extracts. *Phytochem.* **72**, 1814–1820.
12. Schmitt, L. A., Y. Liu, P. A. Murphy and D. F. Birt (2006) Evaluation of the light-sensitive cytotoxicity of *Hypericum perforatum* extracts, fractions, and pure compounds. *J. Agric. Food Chem.* **54**, 2881–2890.
13. Schmitt, L. A., Y. Liu, P. A. Murphy, J. W. Petrich, P. M. Dixon and D. F. Birt (2006) Reduction in hypericin-induced phototoxicity by *Hypericum perforatum* extracts and pure compounds. *J. Photochem. Photobiol., B* **85**, 118–130.
14. Gronquist, M., A. Bezzerides, A. Attygalle, J. Meinwald, M. Eisner and T. Eisner (2001) Attractive and defensive functions of the ultraviolet pigments of a flower (*Hypericum calycinum*). *Proc. Natl Acad. Sci. USA* **98**, 13745–13750.
15. Arellano, J. B. and K. R. Naqvi (2016) Endogenous singlet oxygen photosensitizers in plants. In *Singlet Oxygen: Applications in Biosciences and Nanosciences* (Edited by S. Nonell and C. Flors), pp. 239–269. Royal Society of Chemistry (RSC), Abingdon, Oxfordshire, UK.
16. Ghogare, A. A. and A. Greer (2016) Using singlet oxygen to synthesize natural products and drugs. *Chem. Rev.* **116**, 9994–10034.
17. Helesbeux, J.-J., O. Duval, C. Dartiguelongue, D. Séraphin, J.-M. Oger and P. Richomme (2004) Synthesis of 2-hydroxy-3-methylbut-3-enyl substituted coumarins and xanthones as natural products. Application of the Schenck ene reaction of singlet oxygen with *ortho*-prenylphenol precursors. *Tetrahedron* **60**, 2293–2300.
18. Helesbeux, J.-J., O. Duval, D. Guilet, D. Séraphin, D. Rondeau and P. Richomme (2003) Regioselectivity in the ene reaction of singlet oxygen with *ortho*-prenylphenol derivatives. *Tetrahedron* **59**, 5091–5104.
19. Helesbeux, J.-J., D. Guilet, D. Séraphin, O. Duval, P. Richomme and J. Bruneton (2000) *ortho*-Prenylphenol photooxygenation as a straightforward access to *ortho*-(2-hydroxy-3-methylbut-3-enyl) phenols. *Tetrahedron Lett.* **41**, 4559–4562.
20. Gruszka, J., A. Pawlak and J. Kruk (2008) Tocochromanols, plastoquinol, and other biological prenyllipids as singlet oxygen quenchers —determination of singlet oxygen quenching rate constants and oxidation products. *Free Radic. Biol. Med.* **45**, 920–928.
21. Nowicka, B., J. Gruszka and J. Kruk (2013) Function of plastochromanol and other biological prenyllipids in the inhibition of lipid peroxidation–a comparative study in model systems. *Biochim. Biophys. Acta* **1828**, 233–240.
22. Alberti, M. N. and M. Orfanopoulos (2010) Recent mechanistic insights in the singlet oxygen ene reaction. *Synlett* **7**, 999–1026.
23. Alberti, M. N. and M. Orfanopoulos (2010) Unraveling the mechanism of the singlet oxygen ene reaction: recent computational and experimental approaches. *Chem. Eur. J.* **16**, 9414–9421.
24. Manring, L. E., R. C. Kanner and C. S. Foote (1983) Chemistry of singlet oxygen. 43. Quenching by conjugated olefins. *J. Am. Chem. Soc.* **105**, 4707–4710.
25. Chen, Y.-Z., L.-Z. Wu, L.-P. Zhang and C.-H. Tung (2005) Confined space-controlled hydroperoxidation of trisubstituted alkenes adsorbed on pentasil zeolites. *J. Org. Chem.* **70**, 4676–4681.
26. Griesbeck, A. G., W. Adam, A. Bartoschek and T. T. El-Idreesy (2003) Photooxygenation of allylic alcohols: kinetic comparison of unfunctionalized alkenes with prenol-type allylic alcohols, ethers and acetates. *Photochem. Photobiol. Sci.* **2**, 877–881.

27. Ashen-Garry, D. and M. Selke (2014) Singlet oxygen generation by cyclometalated complexes and applications. *Photochem. Photobiol.* **90**, 257–274.
28. Gibb, B. C. (2016) From steroids to aqueous supramolecular chemistry: An autobiographical career review. *Beilstein J. Org. Chem.* **12**, 684–701.
29. Malek, B., W. Fang, I. Abramova, N. Walalawela, A. A. Ghogare and A. Greer (2016) Ene reactions of singlet oxygen at the air-water interface. *J. Org. Chem.* **81**, 6395–6401.
30. Sparling, B. A., D. C. Moebius and M. D. Shair (2012) Enantioselective total synthesis of hyperforin. *J. Am. Chem. Soc.* **135**, 644–647.
31. Shimizu, Y., S. L. Shi, H. Usuda, M. Kanai and M. Shibasaki (2010) Catalytic asymmetric total synthesis of ent-hyperforin. *Angew. Angew. Chem. Int. Ed.* **49**, 1103–1106.
32. Ang, C. Y., L. Hu, T. M. Heinze, Y. Cui, J. P. Freeman, K. Kozak, W. Luo, F. F. Liu, A. Mattia and M. DiNovi (2004) Instability of St. John's wort (*Hypericum perforatum* L.) and degradation of hyperforin in aqueous solutions and functional beverage. *J. Agric. Food Chem.* **52**, 6156–6164.
33. Brondz, I., T. Greibrokk, P. Groth and A. Aasen (1983) The absolute configuration of hyperforin, an antibiotic from *Hypericum perforatum* L., based on the crystal structure determination of its p-bromobenzoate ester. *Acta Chem. Scand. Ser. A* **37**, 263–265.
34. Brondz, I., T. Greibrokk, P. A. Groth and A. J. Aasen (1982) The relative stereochemistry of hyperforin-an antibiotic from *Hypericum perforatum* L. *Tetrahedron Lett.* **23**, 1299–1300.
35. Bystrov, N., S. R. Gupta, V. Dobrynin, M. Kolosov and B. Chernov (1978) Chemistry of hyperforin. IX. Structure of hyperforin. *Bioorg. Khim.* **4**, 948–955.
36. Flors, C. and S. Nonell (2006) Light and singlet oxygen in plant defense against pathogens: phototoxic phenalenone phytoalexins. *Acc. Chem. Res.* **39**, 293–300.
37. Downum, K. R. (1992) Tansley review no. 43. Light-activated plant defense. *New Phytol.* **122**, 401–420.
38. Gaussian 09, Revision D.01, M. J. Frisch, G. W. T. H. B. Schlegel, G. E. Scuseria, M. A. Robb, J. R. C. G. Scalmani, V. Barone, B. Mennucci, G. A. Petersson, H. N. M. Caricato, X. Li, H. P. Hratchian, A. F. Izmaylov, J. B. G. Zheng, J. L. Sonnenberg, M. Hada, M. Ehara, K. T. R. Fukuda, J. Hasegawa, M. Ishida, T. Nakajima, Y. Honda, O. K. H. Nakai, T. Vreven, J. A. Montgomery, Jr, J. E. Peralta, F. O. M. Bearpark, J. J. Heyd, E. Brothers, K. N. Kudin, V. N. Staroverov, R. Kobayashi, J. Normand, K. Raghavachari, A. Rendell, J. C. Burant, S. S. Iyengar, J. Tomasi, M. Cossi, N. R. J. M. Millam, M. Klene, J. E. Knox, J. B. Cross, V. Bakken, C. A. J. Jaramillo, R. Gomperts, R. E. Stratmann, O. Yazyev, A. J. Austin, R. Cammi, C. Pomelli, J. W. Ochterski, R. L. Martin, K. Morokuma, V. G. Zakrzewski, G. A. Voth, P. Salvador, J. J. Dannenberg, S. Dapprich, A. D. Daniels, O. Farkas, J. B. Foresman, J. V. Ortiz, J. Cioslowski and D. J. Fox (2009). Gaussian, Inc, Wallingford, CT
39. Jensen, F. (2007) *Introduction to Computational Chemistry*, 2nd edn. Wiley, Chichester, UK.
40. Hypercube, Inc. (2009) *HyperChem 8.0.7*. Hypercube, Inc., Gainsville, FL.
41. Connolly, M. L. (1993) The molecular surface package. *J. Mol. Graph. Model.* **11**, 139–14.
42. Connolly, M. L. (1983) Solvent-accessible surfaces of proteins and nucleic acids. *Science* **221**, 709–713.
43. CambridgeSoft Corporation. (2013) *ChemBio3D Ultra 13.0*. CambridgeSoft Corporation, Cambridge, UK.
44. Dennington, R., T. Keith and J. Millam. (2009) *GaussView 5*. Semichem Inc, Shawnee Mission KS.
45. Weiser, J., P. S. Shenkin and W. C. Still (1999) Approximate atomic surfaces from linear combinations of pairwise overlaps (LCPO). *J. Comp. Chem.* **20**, 217–230.
46. Liang, Y.-N., J. Li, Q.-D. Wang, F. Wang and X.-Y. Li (2011) Computational study of the reaction mechanism of the methylperoxy self-reaction. *J. Phys. Chem. A* **115**, 13534–13541.
47. Zhang, P., W. Wang, T. Zhang, L. Chen, Y. Du, C. Li and J. Lü (2012) Theoretical study on the mechanism and kinetics for the self-reaction of $C_2H_5O_2$ radicals. *J. Phys. Chem. A* **116**, 4610–4620.
48. Calabrese, C., A. Maris, L. Evangelisti, L. B. Favero, S. Melandri and W. Caminati (2013) Keto–enol tautomerism and conformational landscape of 1,3-cyclohexanedione from its free jet millimeter-wave absorption spectrum. *J. Phys. Chem. A* **117**, 13712–13718.
49. Pilcher, G., O. G. Parchment, I. H. Hillier, F. Heatley, D. Fletcher, M. A. V. Ribeiro da Silva, M. L. C. C. H. Ferrão, M. J. S. Monte and J. Fang (1993) Thermochemical and theoretical studies on cyclohexanediones. *J. Phys. Chem.* **97**, 243–247.
50. Miyamoto, S., G. R. Martinez, M. H. G. Medeiros and P. Di Mascio (2014) Singlet molecular oxygen generated by biological hydroperoxide. *J. Photochem. Photobiol., B* **139**, 24–33.
51. Miyamoto, S., G. E. Ronsein, F. M. Prado, M. Uemi, T. C. Correa, I. N. Toma, A. Bertolucci, M. C. Oliveira, F. D. Motta and M. H. Medeiros (2007) Biological hydroperoxides and singlet molecular oxygen generation. *IUBMB Life* **59**, 322–331.
52. Miyamoto, S., G. R. Martinez, D. Rettori, O. Augusto, M. H. G. Medeiros and P. Di Mascio (2006) Linoleic acid hydroperoxide reacts with hypochlorous acid, generating peroxyl radical intermediates and singlet molecular oxygen. *Proc. Natl Acad. Sci. USA* **103**, 293–298.
53. Howard, J. and K. Ingold (1968) Self-reaction of sec-butylperoxy radicals. Confirmation of the Russell mechanism. *J. Am. Chem. Soc.* **90**, 1056–1058.
54. Russell, G. A. (1957) Deuterium-isotope effects in the autoxidation of alkyl hydrocarbons. Mechanism of the interaction of peroxy radicals. *J. Am. Chem. Soc.* **79**, 3871–3877.
55. Cantrell, A., D. J. McGarvey, G. Truscott, F. Rancan and F. Bohm (2003) Singlet oxygen quenching by dietary carotenoids in a model membrane environment. *Arch. Biochem. Biophys.* **412**, 47–54.
56. Devasagayam, T. P. A., T. Werner, H. Ippendorf, H. D. Martin and H. Sies (1992) Synthetic carotenoids, novel polyene polyketones and new capsorubin isomers as efficient quenching. *Photochem. Photobiol.* **55**, 511–514.
57. Krasnovskii, A. A. Jr and L. I. Paramonova (1983) Interaction of singlet oxygen with carotenoids: Rate constants of physical and chemical quenching. *Biofizika* **28**, 725–729.
58. Foote, C. S. and R. W. Denny (1968) Chemistry of singlet oxygen. VII. Quenching by β-carotene. *J. Am. Chem. Soc.* **90**, 6233–6235.